Vav3 PROTO-ONCOGENE DEFICIENCY LEADS TO SYMPATHETIC HYPERACTIVITY AND CARDIOVASCULAR DYSFUNCTION

Vincent Sauzeau[1,2,3], María A. Sevilla[1,4], Juan V. Rivas-Elena[4], Enrique de Álava[1,2,3], María J. Montero[1,4], José M. López-Novoa[4], and Xosé R. Bustelo[1,2,3]

[1]Centro de Investigación del Cáncer, [2]Instituto de Biología Molecular y Celular del Cáncer (IBMCC), and [3]Red Temática Cooperativa de Centros de Cáncer, CSIC–University of Salamanca, Campus Unamuno, E–37007 Salamanca, Spain, EU.

[4]Departamento de Fisiología y Farmacología, University of Salamanca, Campus Unamuno, E–37007 Salamanca, Spain, EU

SUPPLEMENTARY NOTE

SUPPLEMENTARY TEXT

The cardiovascular system in *Vav3*$^{-/-}$ mice

As indicated in the main text, *Vav3*$^{-/-}$ mice show extensive cardiovascular remodelling at around 4 months of age. The aorta media wall becomes thicker and disorganized in *Vav3*$^{-/-}$ animals at that time (**Fig. S3a**), showing hyperplasia and hypertrophy of smooth muscle cells (**Fig. 3a**, data not shown) as well as increased deposition of extracellular matrix (**Fig. 1a**). Examination of hearts of *Vav3*$^{-/-}$ animals indicated an increase in the weight of the left ventricle but not of the right one (**Fig. S3b**), leading to a concomitant reduction in the right ventricle/left ventricle weight ratio (**Fig. S3b**). Histological analysis of the left heart ventricle showed a marked hypertrophy of cardiomyocytes (**Fig. S3c,d**). The left ventricle also becomes fibrotic, as determined by both histochemical and biochemical techniques (**Fig. S3c,e**). Treatment of *Vav3*$^{-/-}$ mice with propranolol for 5 weeks prevents the development of the left ventricle fibrosis (**Fig. S3e**), a result that is in agreement with the normal histology of the heart after the same treatment (see main text, **Fig. 3g).** Finally, we observed that hearts from *Vav3*$^{-/-}$ mice did not perform well mechanically, as demonstrated by the lower +dP/dt max values when compared with wild type littermate controls (**Fig. S3f**). Given that +dP/dt max is not usually altered in hypertrophic hearts of hypertensive animals[1], this result suggests that the contractility of the left ventricle is probably altered in *Vav3* knockout animals by as yet unknown mechanisms. The defects in arterial walls and heart were unique for *Vav3*$^{-/-}$ mice, since *Vav3*$^{+/-}$ or *Vav1*$^{-/-}$ animals show no detectable defects (**Fig. S3a,b,d**; data not shown). Further examination of these animals indicated that the tachycardia was not due to intrinsic defects of the sinoauricular node of the heart, because hearts from *Vav3*$^{-/-}$ and control littermates have identical beat frequencies *ex vivo* (data not shown).

SUPPLEMENTARY METHODS

Heart performance assay. A catheter was inserted into the right carotid artery and advanced into the left ventricle under continuous monitoring of the pressure wave form. The penis vein was cannulated with a custom-fashioned polyethylene tube connected to a microinfusion pump. The perfusion was done at a rate of 1 ml/min. The evolution of the left ventricle pressure was recorded and analyzed with a PowerLab system to determine the +dP/dt max. This parameter is a phase index of left ventricular function that is relatively load-independent[2-4].

REFERENCES TO SUPPLEMENTARY TEXT

1. Cingolani, O.H., Yang, X.P., Cavasin, M.A. & Carretero, O.A. Increased systolic performance with diastolic dysfunction in adult spontaneously hypertensive rats. *Hypertension* **41**, 249–254 (2003).
2. Kass, D.A. *et al.* Comparative influence of load versus inotropic states on indexes of ventricular contractility: experimental and theoretical analysis based on pressure-volume relationships. *Circulation* **76**, 1422–1436 (1987).
3. Quinones, M.A., Gaasch, W.H. & Alexander, J.K. Influence of acute changes in preload, afterload, contractile state and heart rate on ejection and isovolumic indices of myocardial contractility in man. *Circulation* **53**, 293–302 (1976).
4. Starling, M.R., Montgomery, D.G., Mancini, G. B. & Walsh, R.A. Load independence of the rate of isovolumic relaxation in man. *Circulation* **76**, 1274–1281 (1987).

Table S1. Analysis of different physiological parameters of 4 month-old *Vav3* and *Vav1* mice.

	Vav3 **$^{+/+}$**	***Vav3*** **$^{+/-}$**	***Vav3*** **$^{-/-}$**	***Vav1*** **$^{-/-}$**
Body weight (g)	29.7 ± 1.5[a]	30.0 ± 0.91	31.2 ± 0.94	32.2 ± 0.94
SAP (mmHg)[b]	86.7 ± 3.8 110 ± 3.0	86.8 ± 1.4 ND	110.5 ± 3.8* 141 ± 7*	82.5 ± 2.1 ND
DAP (mmHg)	61.5 ± 3.7	59.2 ± 3.4	79.6 ± 2.9*	69.2 ± 2.1
MAP (mmHg)	69.9 ± 3.4	68.4 ± 2.7	90.0 ± 3.8*	64.9 ± 3.4
Heart rate (beats/min)	337 ± 16 576 ± 38	334 ± 11 ND	580 ± 24* 774 ± 61*	333 ± 15 ND

[a]Data on blue and black color correspond to the values obtained under awaken and anesthesized conditions, respectively. In the former case,*n* = 13 and 11 for wild type and knockout animals, respectively. In the latter case, *n* = 13, 6, 15, and 8 for *Vav3*$^{+/+}$, *Vav3*$^{+/-}$, *Vav3*$^{-/-}$, and *Vav1*$^{-/-}$ animals, respectively.

[b]SAP, systolic arterial pressure; DAP, diastolic arterial pressure; MAP, mean arterial pressure; ND, not determined.

Figure S1

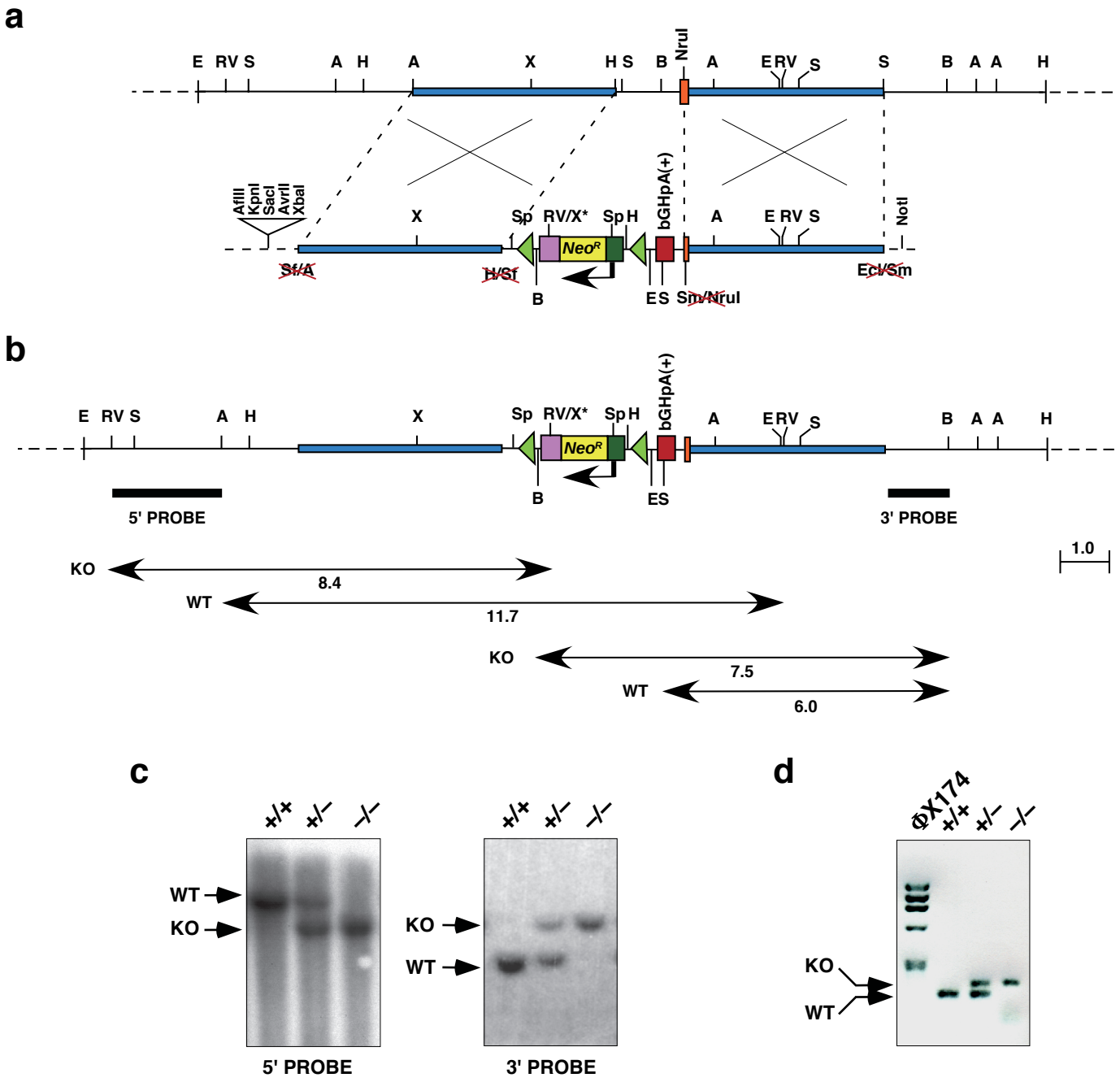
a
E RV S
A H
A
X
H S
B
NruI
A
E RV S
S
B A A
H
AflII
KpnI
SacI
AvrII
XbaI
X
Sp
RV/X*
Sp H
bGHpA(+)
A
E RV S
NotI
Sf/A
H/Sf
B
E S
Sm/NruI
Ec/Sm
b
E RV S
A H
X
Sp
RV/X*
Sp H
bGHpA(+)
A
E RV S
B A A
H
B
ES
5' PROBE
3' PROBE
1.0
KO
8.4
WT
11.7
KO
7.5
WT
6.0
c
+/+
+/−
−/−
WT
KO
5' PROBE
+/+
+/−
−/−
KO
WT
3' PROBE
d
ΦX174
+/+
+/−
−/−
KO
WT

FIGURE S1. Targeted disruption of the mouse *Vav3* gene. (**a,b**) Strategy for the deletion of the promoter region and the 5' end of exon 1 of the *Vav3* locus (a), depiction of the targeting vector (a), and structure of the null *Vav3* allele generated after the homologous recombination event (b). Genomic *Vav3* DNA fragments used for the construction of the two arms of the targeting vector are shown as blue boxes. Exon 1 is highlighted in orange. The *Neo* resistance gene is indicated as a yellow box. The *Pkg-1* promoter used to drive expression of the *Neo* resistance gene is indicated by a dark green box. Arrow indicates the direction of transcription of the *Pkg-1/Neo* construct. *LoxP* sites are shown as green arrowheads flanking the *Neo* gene. The bovine growth hormone polyadenylation signal [bGHpA(+)] is shown as a red box. A, *Acc*65i; B, *Bam*HI; H, *Hind*III; E, *Eco*RI; Ecl, *Ecl*136II; RV, *Eco*RV; S, *Sac*I; Sf, *Sfi*I; Sm, *Sma*I; Sp, *Spe*I; X, *Xba*I; X*, *Xba*I site overlapping with a *Dam* methylation site. Restriction sites that have been eliminated during the ligation of the genomic *Vav3* DNA to the plasmid are crossed in red. The position of the 5' and 3' DNA probes used for the genotyping of animals by Southern blot are shown as black boxes. The diagnostic fragments used in the genotyping of mice by Southern blots with the 5' and 3' DNA probes are indicated at the bottom. Please note that the diagnostic fragments for the wild type allele have to be aligned with the endogenous locus shown in panel a. (**c**) Example of Southern blots with the indicated probes using genomic DNAs from tail biopses that were digested with the restriction enzymes *Eco*RV (left) or *Bam*HI (right). The genotypes of each sample are indicated on top. The position of the WT- and knockout (KO)-specific fragments is indicated by arrows. (**d**) PCR analysis of genomic DNA from tail biopsies. The genotype of each sample is indicated on top. The position of the WT- and knockout-specific PCR fragments is indicated by arrows. ϕX174, lane

containing electrophoresed molecular weight markers derived from the digestion of phage ϕX174 DNA with *Hae*III.

Figure S2

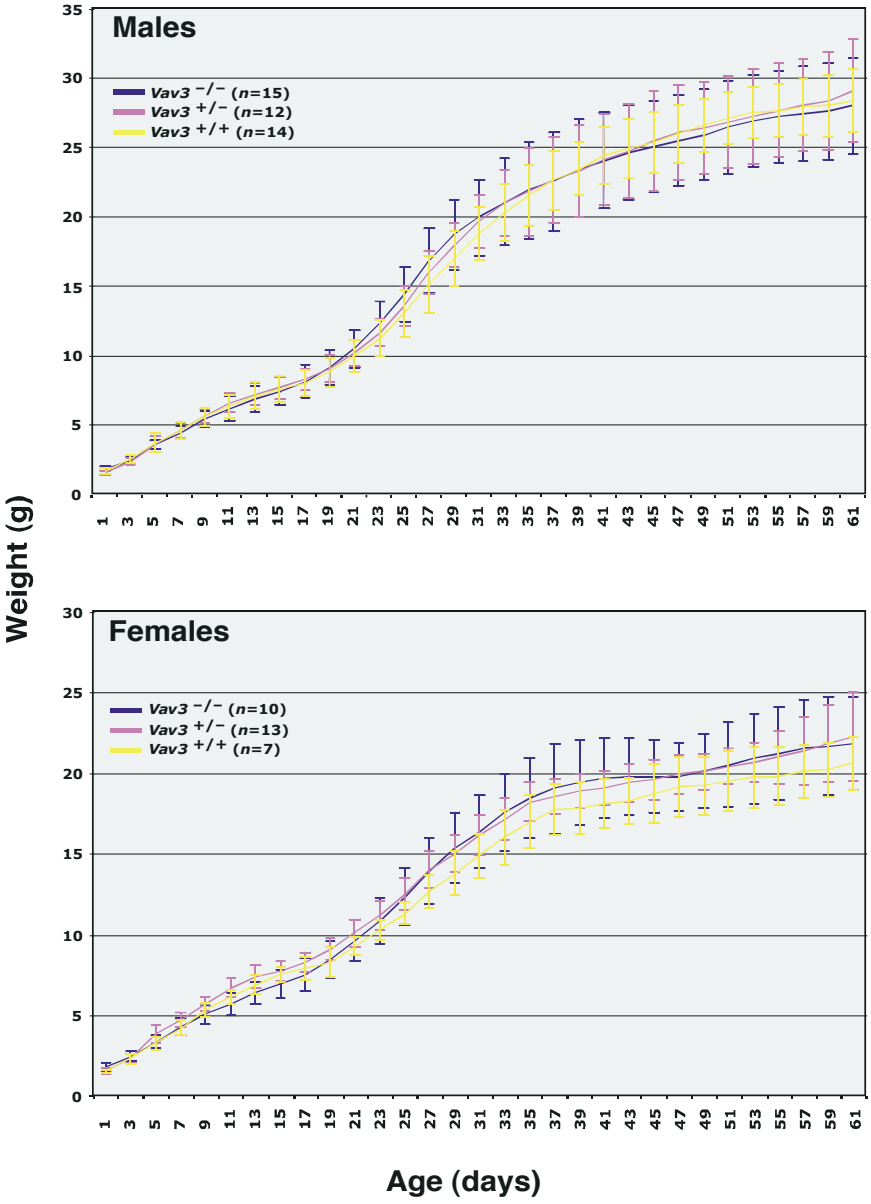
Males
Vav3 −/− (n=15)
Vav3 +/− (n=12)
Vav3 +/+ (n=14)
Females
Vav3 −/− (n=10)
Vav3 +/− (n=13)
Vav3 +/+ (n=7)
Weight (g)
Age (days)

FIGURE S2. Growth rates of *Vav3* knockout animals. Growth curves of male (upper panel) and female (bottom panel) *Vav3*$^{+/+}$ (yellow), *Vav3*$^{+/-}$ (purple), and *Vav3*$^{-/-}$ (blue) mice are shown. Error bars represent the s.e.m.

Figure S3

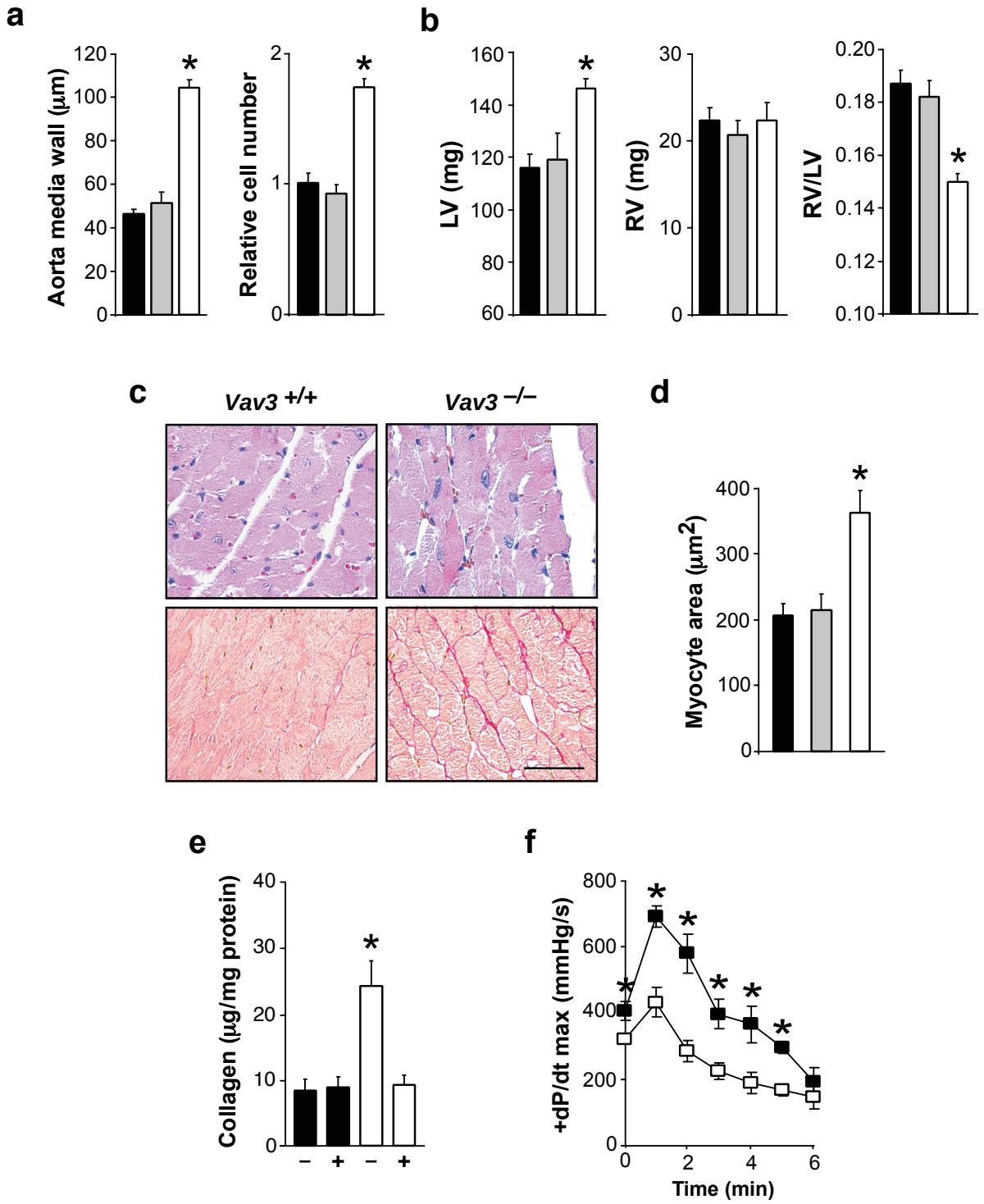
a
Aorta media wall (μm)
120
100
80
60
40
20
0
*
Relative cell number
2
1
0
*
b
LV (mg)
160
140
120
100
80
60
*
RV (mg)
30
20
10
0
RV/LV
0.20
0.18
0.16
0.14
0.12
0.10
*
c
Vav3 +/+
Vav3 −/−
d
Myocyte area (μm2)
400
300
200
100
0
*
e
Collagen (μg/mg protein)
40
30
20
10
0
*
−
+
−
+
f
+dP/dt max (mmHg/s)
800
600
400
200
0
*
*
*
*
*
*
0
2
4
6
Time (min)

FIGURE S3. Analysis of the cardiovascular defects of *Vav3*$^{-/-}$ animals. (**a**) Thickness (left) and relative smooth muscle cell numbers (right) of the aorta media walls of *WT* (black bars), *Vav3*$^{+/-}$ (grey bars), and *Vav3*$^{-/-}$ (white bars) mice (n = 13–15). (**b**) Weight of the left (LV) and right (RV) heart ventricles of *WT* (black bars), *Vav3*$^{+/-}$ (grey bars), and *Vav3*$^{-/-}$ (white bars) mice (n = 13–15). (**c**) Staining with either hematoxylin-eosin (top panels) or Sirius red (bottom panels) of sections from left heart ventricles of mice of the indicated genotypes. Scale bar, 20 μm. (**d**) Quantification of the cardiomyocyte size in the left heart ventricles of *WT* (black bars), *Vav3*$^{+/-}$ (grey bars), and *Vav3*$^{-/-}$ (white bars) mice (n = 8–10). (**e**) Amount of total tissue collagen present in the hearts from *WT* (black bars) and *Vav3*$^{-/-}$ (white bars) mice either untreated (–) or treated (+) with propranolol for 5 weeks (n = 6). (**f**) Determination of the +dP/dt max of the hearts of 4 month-old *WT* (closed squares) and *Vav3*$^{-/-}$ mice (open squares) as indicated in Supplementary Methods (n = 5). Error bars represent the s.e.m. * represents P < 0.01.

Figure S4

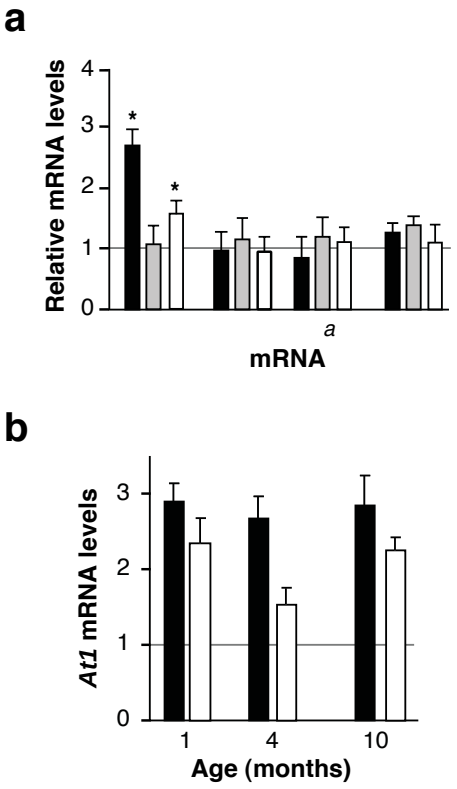
a
Relative mRNA levels
4
3
2
1
0
*
*
a
mRNA
b
At1 mRNA levels
3
2
1
0
1
4
10
Age (months)

FIGURE S4. The status of RAS and endothelin systems in *Vav3*$^{-/-}$ animals. (**a**) Expression levels of *At1*, *At2*, *Eta* and *Etb* mRNAs in aortas (black bars), pulmonary arteries (grey bars) and hearts (white bars) of 4 month-old *Vav3*$^{-/-}$ mice. An arbitrary value of one was given to the expression level of each receptor mRNA in the appropriate control from *Vav3*$^{+/+}$ mice (n = 10–15). (**b**) Expression level of the *At1* mRNA in aortas (black bars) and hearts (white bars) of *Vav3*$^{-/-}$ at the indicated ages. An arbitrary value of one was given to the expression of the *At1* mRNA in the appropriate control sample (n = 7–8). In a and b, error bars represent the s.e.m and * indicates P <0.01.

Figure S5

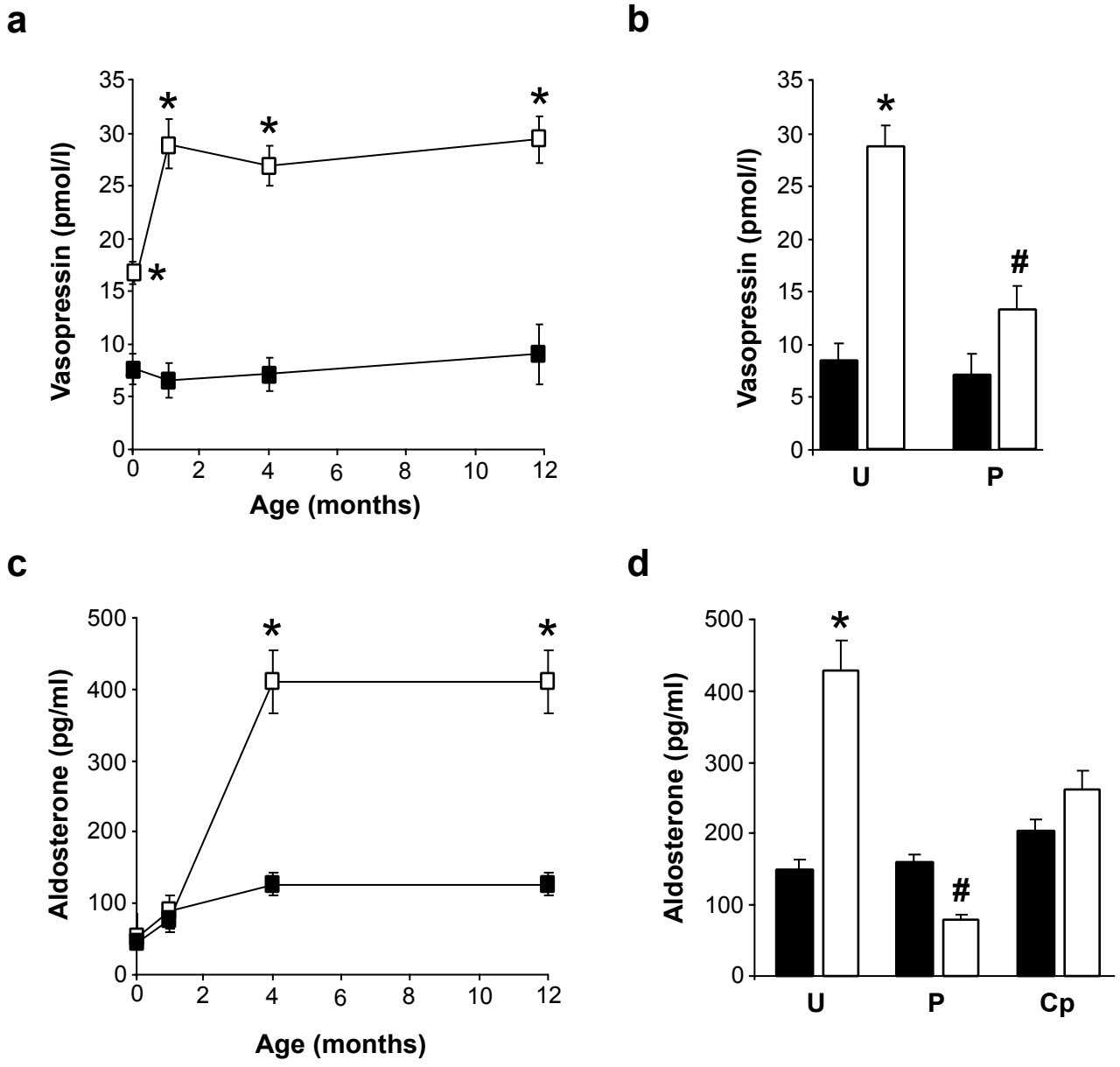

FIGURE S5. Vasopressin and aldosterone levels in *Vav3*$^{-/-}$ animals. **(a,c)** Plasma levels of vasopressin (a, $n \geq 5$) and aldosterone (c, $n \geq 5$) in *WT* (closed squares) and *Vav3* null (open squares) mice of the indicated ages. **(b,d)** Effect of propranolol (b,d) or captopril (d) on the plasma levels of vasopressin (b, $n = 5$) and aldosterone (d, $n = 5$) in *WT* (closed bars) and *Vav3* null (open bars) mice. U, untreated; P and Cp, propranolol- and captopril-treated animals, respectively. Error bars represent the s.e.m. # and * represent $P < 0.05$ and 0.01, respectively.

MICRORNA

Silence of the P bodies

Recent studies have indicated that microRNAs (miRNAs) can reduce the levels of their target transcripts and the expression of the translated proteins. Elisa Izaurralde and colleagues now provide further evidence that *Drosophila melanogaster* miRNAs silence gene expression by these two mechanisms, which both require the processing (P)-body component GW182.

> “The present findings place GW182 firmly in the miRNA-silencing pathway…”

Izaurralde and co-workers compared the expression profiles of GW182-depleted cells with those of argonaute-1 (AGO1)-depleted cells (AGO1 mediates gene silencing by miRNAs in *D. melanogaster*). The profiles were strikingly similar, which indicates that these proteins regulate a common set of mRNAs and are therefore likely to function in the same pathway.

By transfecting cells with a GW182 fusion construct that binds with high affinity to a luciferase reporter mRNA target, the authors demonstrated that GW182 silences expression of the bound transcripts. In cells that were depleted of AGO1, GW182 still silenced reporter expression, bypassing the requirement for AGO1, which indicates that GW182 functions downstream of AGO1. The authors also identified the N-terminal domain of GW182 as the AGO1-binding region.

Tethering of GW182 to the reporter mRNA caused a marked reduction in the levels of reporter mRNA, which could not account fully for the observed decrease in luciferase activity. This therefore indicated that GW182-mediated silencing can occur by two mechanisms — repression of protein expression and mRNA degradation. By monitoring the levels of reporter mRNA over time in the presence of GW182, the authors noticed a decrease in the half-life of the mRNA. The mRNAs also shortened slightly over time, which implied that deadenylation had occurred. Further tethering assays revealed that the CCR4–NOT deadenylase complex was required for GW182-mediated mRNA degradation. The DCP1–DCP2 decapping complex was similarly required for mRNA decay by GW182.

Using various reporter constructs that comprised endogenous *D. melanogaster* mRNA targets that are each inhibited by a corresponding miRNA, the authors showed that miRNAs trigger reductions in mRNA levels to different extents. As expected, target-mRNA levels were upregulated and expression levels increased in cells that were depleted of GW182. Silencing of one of the reporter transcripts occurred mainly at the translational level and, as a result, depletion of deadenylase or decapping components did not restore luciferase expression. It is currently unclear however how GW182 represses translation.

The present findings place GW182 firmly in the miRNA-silencing pathway; nevertheless, several questions remain open. Is miRNA-mediated translational repression the cause of mRNA degradation or are these two independent mechanisms? And what determines the degree of mRNA decay and the regulation of gene expression at the level of translation or mRNA stability?

Arianne Heinrichs

ORIGINAL RESEARCH PAPER
Behm-Ansmant, I. *et al.* mRNA degradation by miRNAs and GW182 requires both CCR4:NOT deadenylase and DCP1:DCP2 decapping complexes. *Genes Dev.* 30 June 2006 (doi:10.1101/gad.1424106)

Web watch

RECIPES FOR RESULTS

- http://www.natureprotocols.com/

We've all spent frustrating hours searching through the methods sections of articles to find the best way to do our experiments. And we've leafed through cookbooks, trying to find that perfect recipe to impress that special someone. Now *Nature Protocols*, which launched in June 2006, has combined these two processes, switched the pinch of frustration for a helping of interactivity, and provided an online, comprehensive, recipe-like collection of biological and biomedical protocols.

Nature Protocols articles are commissioned and peer reviewed, and cover diverse subjects, guaranteeing that there is something for everyone. By the end of 2006, *Nature Protocols* aims to have over 400 published protocols. Alongside the commissioned protocols, the website presents the 'Protocols Network', in which anyone can freely upload their laboratory procedures.

Through an interactive forum, comments, advice and constructive criticism can be read, and written, for all of the protocols on the site, ensuring that protocols are up to date and that you are well informed. The website is searchable, and protocols are linked to other relevant procedures and grouped into categories to allow for easy browsing. And another helpful feature, the 'Tools & Reagents' subsection, details how to make up many commonly used reagents.

Access to the full content of *Nature Protocols* is available through an institutional site license, whereas the interactive access to the 'Protocols Network' is free. So whether you are having troubleshooting difficulties, or are designing your next ground-breaking experiment, log on to *Nature Protocols* and find the perfect protocol that will help you get the results you need to impress that special peer reviewer.

Asher Mullard

MECHANISMS OF DISEASE

VAV proteins get busy

> "Now, the role of VAV proteins is expanding, as two reports show that these proteins also have important functions in other tissues."

The function of VAV proteins has been extensively characterized downstream of immune-response receptors. Now, the role of VAV proteins is expanding, as two reports show that these proteins also have important functions in other tissues. Sauzeau *et al.* found that the loss of VAV3 promotes the gradual development of hypertension and cardiovascular dysfunction in mice, whereas a report by Hunter and colleagues indicates a role for VAV2 and VAV3 as regulators of angiogenesis *in vivo*.

The three members of the VAV family (VAV1–3) are guanine nucleotide-exchange factors (GEFs) for Rho-family GTPases, and they have similar regulatory and catalytic properties. By modulating the activities of Rho and Rac, they regulate the organization of the cytoskeleton. Despite the widespread localization of VAV2 and VAV3 in mouse tissues, most studies have focused on VAV function in the immune system.

To look for other functions of VAV3, Sauzeau and colleagues generated *Vav3*-knockout mice. These mice had high systolic and diastolic blood pressures. In addition, these mice had tachycardia and cardiovascular defects, reminiscent of human defects associated with hypertension. In an attempt to identify whether the renin–angiotensin system (RAS) or the endothelin system — two essential physiological circuits that are involved in hypertension — mediate

CYTOSKELETON

Measuring growth

In *Nature*, Dogterom and colleagues now describe a new optical-tweezers-based method that can be used to observe the assembly dynamics of individual microtubules at molecular resolution. Microtubules — a crucial part of the cytoskeleton in all eukaryotic cells — are dynamic protein polymers that are known to self-assemble from tubulin dimers. However, there has been a lack of information about the molecular events that underlie the growth and shrinkage of microtubules, because studies *in vitro* and *in vivo* have been limited to measurements of average growth and shrinkage rates.

> "…a new optical-tweezers-based method that can be used to observe the assembly dynamics of individual microtubules…"

To obtain information on microtubule dynamics at the resolution of single tubulin dimers (8 nm), Dogterom and co-workers developed a technique based on optical tweezers that allows dynamic microtubule plus ends to grow and shrink against a microfabricated barrier. A bead was attached to an axoneme — a rigid bundle of multiple stabilized microtubules — and the bead–axoneme construct was suspended in an optical trap near a barrier. Microtubule growth was initiated by the addition of tubulin and GTP, and microtubule growth was measured by monitoring bead displacement.

In the presence of tubulin and GTP, the authors observed 20–30-nm stepwise increases in microtubule length. This is significantly larger than the 8-nm size of a tubulin dimer, which indicates that microtubule assembly might not always occur through the addition of individual dimers. When the microtubule-associated protein

the *Vav3*$^{-/-}$ defects, the authors measured the levels of several molecules. They found high levels of renin, angiotensin-converting enzyme and angiotensin II, which indicates that the RAS system contributes to the development of the cardiovascular dysfunction.

Although the molecular mechanism of *Vav3*$^{-/-}$-mediated hypertension remains to be investigated, Sauzeau and colleagues also found that the levels of the catecholamines (adrenaline, noradrenaline and dopamine) of the sympathetic nervous system (SNS) were elevated from the time of birth in the plasma of *Vav3*$^{-/-}$ mice. Treatment with a non-selective β-adrenergic-receptor inhibitor blocked the development of hypertension, tachycardia and heart fibrosis, indicating that the *Vav3*$^{-/-}$ cardiovascular defects are due to an SNS-dependent stimulation of RAS.

The second report highlights a potential mechanism for Vav protein function in another non-haematopoietic process: angiogenesis. Using a yeast two-hybrid screen, Hunter *et al.* identified VAV3 as a binding partner of the EphA2 receptor tyrosine kinase, which is an important regulator of angiogenesis. Deletion-mutant analysis in conjunction with immunoprecipitations showed that both VAV2 and VAV3 are recruited to phosphorylated EphA2 receptors in mammalian cells after treatment with the EphA2 ligand ephrin-A1.

Morphological analysis in mouse embryonic fibroblasts showed that *Vav2- Vav3*-deficient cells have impaired spreading on ephrin-A1-coated surfaces. Furthermore, activation of VAV2 and VAV3 by the EphA2 receptor induced Rac1 GTPase activity and cell migration of endothelial cells. Based on the defects of *Vav2- Vav3*-deficient cells, the authors then examined *Vav2*$^{-/-}$ *Vav3*$^{-/-}$ mice and found that loss of both VAV2 and VAV3 is required for ephrin-A1-mediated angiogenic remodelling *in vivo*.

Not bad for a family of proteins that was thought 'only' to function in the immune system. The analysis of the *Vav2*$^{-/-}$ *Vav3*$^{-/-}$ mutant mice should provide further insights into the functions of these molecules in various tissues.

Ekat Kritikou

ORIGINAL RESEARCH PAPERS Sauzeau, V. *et al.* Vav3 proto-oncogene deficiency leads to sympathetic hyperactivity and cardiovascular dysfunction. *Nature Med.* 11 June 2006 (doi:10.1038/nm1426) | Hunter, S. G. *et al.* Essential role of Vav family guanine nucleotide exchange factors in EphA receptor-mediated angiogenesis. *Mol. Cell. Biol.* **26**, 4830–4842 (2006)

XMAP215 was included in the assay, the growth was markedly enhanced such that rapid length increases of 40–60 nm were observed. These observations indicate that "small tubulin oligomers are able to add directly to growing microtubules and that XMAP215 speeds up microtubule growth by facilitating the addition of long oligomers." In the future, it will be interesting to use this technique to investigate how other types of microtubule-associated protein regulate microtubule dynamics.

Rachel Smallridge

ORIGINAL RESEARCH PAPER Kerssemakers, J. W. J. *et al.* Assembly dynamics of microtubules at molecular resolution. *Nature* 25 June 2006 (doi:10.1038/nature04928)
FURTHER READING Howard, J. & Hyman, A. A. Dynamics and mechanics of the microtubule plus end. *Nature* **422**, 753–758 (2003)
WEB SITE
Institute for Atomic and Molecular Physics, Dutch Foundation for Fundamental Research on Matter: http://www.amolf.nl

IN BRIEF

DNA REPLICATION

Live-cell imaging reveals replication of individual replicons in eukaryotic replication factories.

Kitamura, E. *et al. Cell* **125**, 1297–1308 (2006)

The authors developed a new assay to study the dynamics of DNA replication in single cells using time-lapse microscopy. Their findings support the long-standing hypothesis that sister replication forks that are generated from the same origin remain associated with each other in a replication factory during replication. In addition, the formation of replication factories was found to depend on Cdc6, which is required for DNA replication initiation. The authors therefore propose that replication-factory formation is a consequence of DNA replication.

DNA REPAIR

Histone modification-dependent and -independent pathways for recruitment of checkpoint protein Crb2 to double-strand breaks.

Du, L.-L. *et al. Dev. Cell* **20**, 1583–1596 (2006)

Live immunofluorescence-microscopy studies were combined with genetic analysis to investigate the role of the *Schizosaccharomyces pombe* protein Crb2, a mediator of the DNA-damage response. Du and co-workers show that Crb2 relocalizes to sites of DNA double-strand breaks and that this relocalization requires the modification of histones H2 and H4. However, neither of these modifications is required for Crb2 to carry out its mediator function. A second recruitment mechanism is independent of histone modifications, and such dual recruitment mechanisms are thought to be a common feature of DNA-damage-checkpoint mediators.

MORPHOGENESIS

Coordinated cell-shape changes control epithelial movement in zebrafish and *Drosophila*.

Köppen, M. *et al. Development* **133**, 2671–2681 (2006)

In this study, the authors show that the process of spreading the outer epithelium of the zebrafish embryo over the yolk cell surface and the underlying cells requires the localized recruitment of actin and myosin-2 in the yolk cytoplasm. This process also requires the Ste20-like kinase Msn1, an orthologue of *Drosophila melanogaster* Misshapen. Similarly, these three proteins are needed during dorsal closure in *D. melanogaster*. Together, these data hint at the existence of a conserved mechanism that coordinates cell-shape changes during epithelial morphogenesis.

NUCLEAR TRANSPORT

Flexible phenylalanine–glycine nucleoporins as entropic barriers to nucleocytoplasmic transport.

Lim, R. Y. H. *et al. Proc. Natl Acad. Sci. USA* **103**, 9512–9517 (2006)

The nature of the selective barrier-gate of nuclear pore complexes (NPCs) is poorly understood. About 30% of the nucleoporins, which make up the NPC, contain a domain that is enriched in Phe–Gly (FG) repeats. Tethering of the FG domain of nucleoporin Nup153 to the surface of so-called nanodots showed that this domain is unfolded and flexible. Atomic force microscopy analysis showed that it forms brush-like conformations, which function as a repulsive entropic barrier at the nuclear pore.